Advances in Engineering Innovation (2024) Volume 9 EWA Publishing
Published online: 31 July 2024 DOI: 10.54254/2977-3903/9/2024096

Fault diagnosis of railway freight car rolling bearings based on ACMD and improved MCKD

Tang Wuchu [1], Jia Zhenlin [1,*], Lai Dongmei [1]

[1] Dalian Jiaotong University, 794 Huanghe Road, Shahekou District, Dalian, Liaoning

[*] 2847022514@qq.com

Abstract. To address the issue of accurately extracting fault characteristic information of railway freight car bearings under noisy conditions, this paper proposes a fault diagnosis method based on Adaptive Chirp Mode Decomposition (ACMD) and an optimized Maximum Correlation Kurtosis Deconvolution (MCKD) using a Sparrow Search Algorithm Combining Sine-Cosine and Cauchy Mutation (SCSSA). Firstly, ACMD is used to decompose and reconstruct the original fault signal to obtain several Intrinsic Mode Functions (IMFs). Then, the IMFs are filtered according to the Gini coefficient indicator, with the IMF having the largest Gini coefficient selected as the optimal component. Secondly, the SCSSA is employed to iteratively optimize the filter length L, fault signal period T, and displacement parameter M in the MCKD algorithm, determining the optimal parameter combination for MCKD. This avoids the limitations of manual settings and enhances the accuracy of fault diagnosis. The optimized MCKD is then applied to the optimal component, and deconvolution is performed using maximum correlation kurtosis as the criterion to extract fault characteristic information through its envelope spectrum. To verify the effectiveness and generalizability of the proposed method, simulations, experimental signals from the Case Western Reserve University Bearing Center, and actual measured signals from railway freight car bearing 353130B are used to analyze inner ring faults. The experimental results demonstrate that the method can accurately extract fault characteristic information of railway freight car bearings under noise interference and identify the fault type.

Keywords: Adaptive Chirp Mode Decomposition (ACMD), Sparrow Search Algorithm Combining Sine-Cosine and Cauchy Mutation (SCSSA), Maximum Correlation Kurtosis Deconvolution (MCKD), railway freight car bearings, fault diagnosis

1. Introduction

As a critical component of railway freight cars, bearings are closely related to the operational status and safety of the vehicles [1]. Ensuring safe vehicle operation and reducing the likelihood of accidents hinge on accurately identifying bearing fault characteristics. Fault signals are characterized by nonlinearity and non-stationarity, and are often contaminated with various types of noise. Fault characteristics are typically weak and frequently obscured by strong background noise, making accurate fault identification very challenging. Therefore, it is crucial to accurately extract rolling bearing fault characteristics, reduce noise interference, and improve the signal-to-noise ratio. Selecting appropriate methods for signal processing is essential. Many experts have proposed signal analysis techniques. The Empirical Mode Decomposition (EMD) technique [2] has good adaptability but still falls short in terms of decomposition quality and is accompanied by issues such as endpoint effects and mode mixing [3]. The Variational Mode Decomposition (VMD) technique proposed by Dragomiretskiy [4] and others can effectively address endpoint effects and mode mixing problems and has been applied in mechanical fault monitoring. Despite this, the VMD algorithm is influenced by parameters such as the number of decomposition layers and penalty factors. When the type of fault and characteristic frequencies are unknown, manually setting parameters based on experience limits the applicability of this technology in fault diagnosis [5]. To address this issue, suitable optimization algorithms and fitness functions should be adopted to adaptively adjust periodic parameters to ensure the accuracy and applicability of parameter settings. Chen [6] proposed Adaptive Chirp Mode Decomposition (ACMD), which has the ability to decompose signals adaptively and thereby extract fault characteristics more effectively. In further developments, a blind deconvolution method based on periodic information was proposed. Tang Guiji [7] and others introduced the Maximum Correlation Kurtosis Deconvolution (MCKD) algorithm, using maximum correlation kurtosis as the objective function. By empirically adjusting parameters such as filter length L and fault period T, and utilizing deconvolution iteration to highlight fault characteristics in the signal, the algorithm performs exceptionally well. These methods have effectively extracted and identified early fault characteristics in bearings.

In determining the parameters of the MCKD algorithm, parameter selection is crucial. Relying solely on traditional manual experience has certain limitations and cannot ensure the accuracy of the algorithm. To address this issue, this paper employs the Sparrow Search Algorithm Combining Sine-Cosine and Cauchy Mutation (SCSSA) [8], which optimizes parameters such as filter length L, fault period T, and displacement parameter M, compared to the Particle Swarm Optimization (PSO) algorithm proposed by Zhang Jun [9] and others. This approach introduces a new method for parameter optimization, enhancing global search capabilities and effectively avoiding issues with local extrema [10], thereby providing a degree of adaptability to the fault diagnosis method. Considering the actual operating conditions of railway freight car bearings, noise interference, and different parameter selections, this paper proposes a railway freight car rolling bearing fault diagnosis method combining ACMD decomposition and SCSSA-optimized MCKD. Firstly, ACMD is applied for the decomposition and reconstruction preprocessing of fault signals to reduce the interference from irrelevant components and noise. Subsequently, SCSSA optimizes the relevant parameters of MCKD to ensure improved deconvolution performance of the optimized MCKD. Finally, fault characteristic extraction and diagnosis of railway freight car bearings can be achieved through envelope demodulation.

2. Related theories

2.1. Basic principles

2.1.1. Adaptive Chirp Mode Decomposition (ACMD)

Adaptive Chirp Mode Decomposition (ACMD) is an adaptive decomposition method that decomposes non-stationary vibration signals into several components without requiring the number of statistical components to be predetermined. Since mechanical fault signals exhibit nonlinearity and non-stationarity [11] and often contain multiple components, they can be modeled as signals with amplitude modulation and frequency modulation.

$$y(t) = \sum_{k=1}^{K} y_k(t) = \sum_{k=1}^{K} A_k \cos\left[2\pi \int_0^1 f_k(s) + \phi_k\right] \tag{1}$$

where k denotes the number of signal components; $A_k(t)$, $f_k(t)$, and ϕ_k represent the instantaneous amplitude (IA), instantaneous frequency (IF), and initial phase, respectively.

After demodulation, equation (1) can be rewritten as:

$$y(t) = \sum_{k}^{K} \left\{\alpha_k(t) \cos\left[2\pi \int_0^t \tilde{f}_k(s) ds\right] + \beta_k(t) \sin\left[2\pi \int_0^t \tilde{f}_k(s) ds\right]\right\} \tag{2}$$

where $\alpha_k(t)$ and $\beta_k(t)$ are the demodulated signals, which can be further expressed by equations (3) and (4):

$$\alpha_k(t) = A_k \cos\left\{2\pi \int_0^t \left[f_k(s) - \tilde{f}_k(s)\right] ds + \phi_k\right\} \tag{3}$$

$$\beta_k(t) = A_k \sin\left\{2\pi \int_0^t \left[f_k(s) - \tilde{f}_k(s)\right] ds + \phi_k\right\} \tag{4}$$

where $\tilde{f}_k(s)$ represents the frequency response function of the demodulation.

Therefore, the instantaneous amplitude of the signal in equation (2) can be estimated using equation (5):

$$A_k = \sqrt{\alpha_k^2(t) + \beta_k^2(t)} \tag{5}$$

When $f_k(s) = \tilde{f}_k(s)$ denotes a constant signal frequency, it can be demodulated into an amplitude-modulated signal with the narrowest bandwidth, alternating between updating the demodulated signal and frequency function. The initial signal $F_t(t)$ is decomposed into:

$$F_t(t) = \sum_{i=1}^{K} \tilde{F}_i(t) + R_K(t) \tag{6}$$

The algorithm's termination condition is set such that when the energy ratio of the remaining components to the initial signal reaches a threshold, this threshold is used as the termination criterion to control the accuracy and efficiency of the algorithm. Once the preset threshold is reached, the demodulation result is considered sufficiently close to the original signal, and the algorithm stops running.

2.2. Principle of reconstructed signal based on Gini Index (GI)

The Gini Index (GI) is an excellent sparse index with strong robustness against random noise interference [12]. The Gini coefficient ranges from 0 to 1, with higher values indicating greater contribution of the feature to fault classification. By selecting the feature with the highest Gini coefficient as the basis for classification, effective fault classification can be achieved. The Gini coefficient is defined as:

$$GI = 1 - 2\sum_{n=1}^{N} \frac{\vec{t}_{(n)}}{\|t\|_1} \left(\frac{N-n+0.5}{N}\right) \tag{7}$$

where $\|t\|_1$ is the 1-norm of t, t is the squared envelope (SE) of the signal, $\vec{t}$ is the vector of t sorted in ascending order, and N is the total length of the signal. When the signal has a high GI value, the impact effect is more pronounced. The GI index of each component is calculated and ordered by the reconstruction function. During iteration, the GI index of signal components added pairwise is computed, and the maximum value is identified. If this value is greater than the current GI value of the signal component, indicating that merging results in a higher GI index, the two signals are merged [13], and the GI index is updated. This process continues until the GI value no longer increases after any two components are merged. By selecting the component with the highest GI value, the signal-to-noise ratio of the signal after ACMD decomposition is better improved.

2.3. Principle of Maximum Correlation Kurtosis Deconvolution (MCKD)

During the transmission of fault signals, they undergo a series of convolution operations before being received by vibration sensors. The signal $\vec{x} = [x_1 x_2 \dots x_K]^T$ received by the sensor is the result of convolving the fault signal $\vec{m}$ with the noise function $\vec{n}$, expressed as:

$$\vec{x} = \vec{h}_m * \vec{m} + \vec{h}_n * \vec{n} \tag{8}$$

The MCKD algorithm [14] performs deconvolution of the received vibration signal by finding an optimal filter. The goal is to make the filtered signal approximate the fault impact signal, with maximum correlation kurtosis [15] as the evaluation criterion:

$$\vec{y} = \vec{f} * \vec{x} = \sum_{l=1}^{L} f_l\, x_{i-l+1} \tag{9}$$

where $\vec{y}$ represents the filtered fault impact signal, $\vec{x}$ is the sensor-received signal, L is the filter length parameter $l \in [0, L]$, and $*$ denotes convolution. The definition of maximum correlation kurtosis is given by:

$$CK_M(T) = \frac{\sum_{i=1}^{I}(\prod_{m=0}^{M} y_{i-mT})^2}{(\sum_{i=1}^{N} y_i^2)^{M+1}} \tag{10}$$

where M is the displacement parameter, T is the fault signal period, and I is the number of sampling points.

The correlated kurtosis more broadly considers the periodic characteristics of impulse signals compared to kurtosis, making it more effective in evaluating periodic impulse components. Unlike kurtosis [16], which is only sensitive to some sharp impulse signals, correlated kurtosis can comprehensively evaluate the characteristics of impulse signals. Its objective function is:

$$\max_{\vec{f}} C\,K_M(T) = \max_{\vec{f}} \frac{\sum_{i=1}^{N}(\prod_{m=0}^{M} y_{i-mT})^2}{(\sum_{i=1}^{N} y_i^2)^{M+1}} \tag{11}$$

where $\vec{f}$ is the filter parameter, and $\vec{f} = [f_1 f_2 \dots f_3]^T$. By taking the derivative of the numerator and the denominator, we obtain

$$\frac{d}{df_k} CK_M Nmerator = 2\sum_{i=1}^{I}\left[(\prod_{m=0}^{M} y_{i-mT})^2 \left(\sum_{m=0}^{M} \frac{x_{i-mT-k+1}}{y_{i-mT}}\right)\right]$$

$$\frac{d}{df_k} CK_M Denominator = 2(M+1)\|\vec{y}\|^{2M} \sum_{i=1}^{I} y_i x_{i-k+1}$$

$$\frac{d}{df_k} CK_M(T) = 2\|\vec{y}\|^{-2M-2} \sum_{i}^{I}\left[(\prod_{m=0}^{M} y_{i-mT})^2 (\sum_{m=0}^{M} \frac{x_{i-mT-k+1}}{y_{i-mT}})\right] - 2(M+1)\|\vec{y}\|^{-2M-4} \sum_{i=1}^{I} y_i x_{i-k+1} = 0 \tag{12}$$

Substituting the variable k, the filter parameter $\vec{f}$ can be expressed as:

$$\vec{f} = \frac{\|\vec{y}\|^2}{2\|\vec{\beta}\|^2} (\vec{x}_0 \vec{x}^T)^{-1} \sum_{m=0}^{M} (\vec{x}_{mT} \vec{\alpha}_m) \tag{13}$$

2.4. Optimization process

This paper primarily uses the Sparrow Search Algorithm Combining Sine-Cosine and Cauchy Mutation (SCSSA) [8] to address issues such as population diversity loss and local extremum problems that may occur in the later stages of optimization with the standard Sparrow Search Algorithm (SSA). In position updates, a sine-cosine strategy [17] is introduced, which is improved by increasing the decremental search factor and weight factor to balance local exploitation and global exploration. Additionally, the Cauchy mutation mechanism is employed to perturb the optimal solutions in follower position updates, thereby expanding the search range, avoiding local extrema, and enhancing global optimization capabilities [18].

The update rules for the discoverers and followers' positions are as follows:

$$X_{i,j}^{t+1} = \begin{cases} \omega \cdot X_{i,j}^{t} + r_1' \cdot \sin r_2 \cdot \left| r_3 \cdot X_{best}^{t} - X_{i,j}^{t} \right|, R_2 < ST \\ \omega \cdot X_{i,j}^{t} + r_1' \cdot \cos r_2 \cdot \left| r_3 \cdot X_{best}^{t} - X_{i,j}^{t} \right|, R_2 \geq ST \end{cases}$$

$$X_{i,j}^{t+1} = X_{best}(t) + cauchy(0,1) \oplus X_{best}(t) \tag{14}$$

In the equation, r_1 is the step size search factor, α is the constant 1, t is the number of iterations, η is the adjustment coefficient, $\eta \geq 1$, ω is the nonlinear weight factor, r_2 is a random number in the range $[0,2\pi]$ that determines the movement distance of the sparrow; r_3 is a random number in the range $[0,2\pi]$, $cauchy(0,1)$ is the standard Cauchy distribution function; and $\oplus$ denotes multiplication.

3. Fault diagnosis process

The fault diagnosis method based on ACMD-SCSSA-MCKD is implemented through the following steps, as shown in the flowchart.

Step 1: First, decompose the original signal using ACMD to obtain several intrinsic mode functions (IMFs). Calculate the Gini Index (GI) for each IMF, and select the IMF with the highest GI as the optimal component after reconstruction.

Step 2: The optimal component undergoes parameter optimization for MCKD $[L, T, M]$, determining the best influencing parameters $[L_0, T_0, M_0]$. The optimization algorithm is the sparrow search algorithm combined with sine-cosine and Cauchy mutation, and the optimal parameters are fed back into the MCKD algorithm for deconvolution of the optimal component.

Step 3: Perform envelope spectrum analysis on the deconvoluted optimal IMF to complete the fault diagnosis.

4. Weak fault simulation verification of rolling bearing inner ring

4.1. Construction of simulation signal

To verify the effectiveness of the method proposed in this paper, a fault periodic simulation signal affected by background noise is constructed as follows:

$$\begin{cases} x(t) = \sum_{\kappa} A_{\kappa} h(t - \kappa T_1 - \tau_{\kappa}) + n(t) \\ A_{\kappa} = A_0 \sin(2\pi f_r t) + 1 \\ h(t) = \exp(-Ct) \sin(2\pi f_n t) \\ x(t) = y(t) + n(t) \end{cases} \tag{24}$$

where: Amplitude A_0= 0.500, rotational frequency f_r=25 Hz, decay coefficient C = 800, resonance frequency f_n=4000 Hz, inner ring fault frequency f_i=$1/T_1 = 110Hz$, and $n(t)$ represents Gaussian white noise with a level of -5 dB. The sampling frequency is 12,800 Hz, and the number of analysis points is 8192.

4.2. Simulation results

From the simulation analysis, it is observed that the fault features in the signal are obscured by noise. Additionally, there are no distinct fault information features in the envelope spectrum. This indicates that under background noise conditions, extracting fault information effectively is quite challenging.

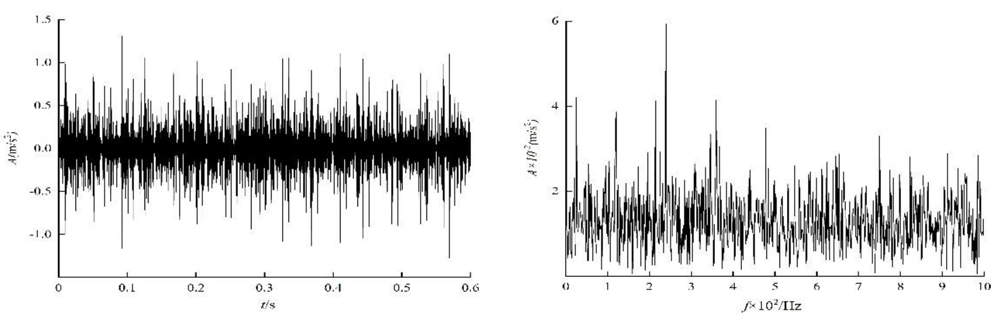

(a) Original Time-Domain Waveform of Simulation Signal
(b) Original Envelope Spectrum of Simulation Signal

Figure 1. Waveform and Envelope Spectrum of Simulation Signal

First, ACMD is used to decompose the original signal to obtain several components. The reconstruction function is then applied, and the IMF with the highest Gini Index, IMF8, is selected as the optimal component.

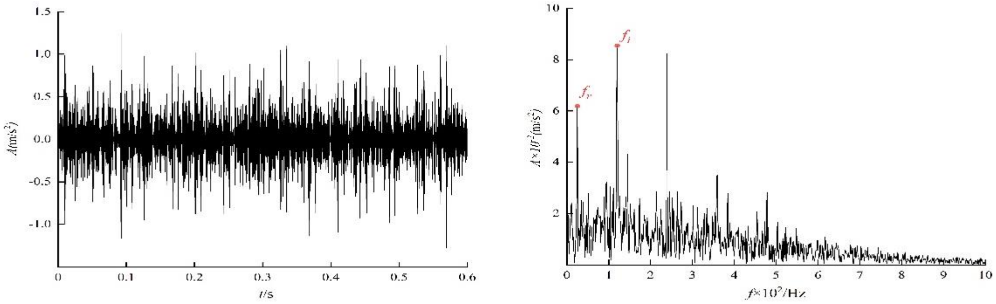

(a) Time-Domain Waveform of Optimal Component of Simulation Signal
(b) Envelope Spectrum of Optimal Component of Simulation Signal

Figure 2. Time-Domain Waveform and Envelope Spectrum of Optimal Component of Simulation Signal

After ACMD decomposition, the time-domain waveform and envelope spectrum of the final component are shown in Fig.2. Compared to Fig.3, the random interference impact component is significantly reduced in Fig.4, and it exhibits the time-domain waveform characteristics of inner ring faults. Additionally, the envelope spectrum highlights the characteristic frequencies of the inner ring fault, indicating potential inner ring damage in the bearing.

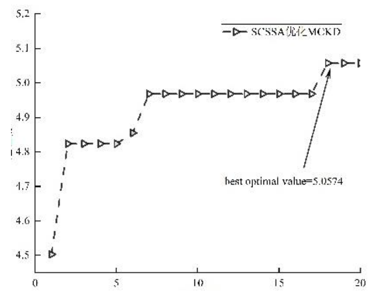

(a) SCSSA Optimization Process

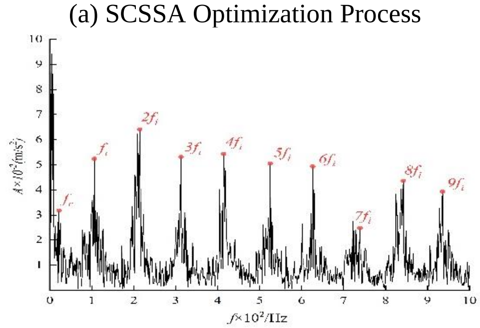

(b) Envelope Spectrum of Optimal Component After the Proposed Method

Figure 3. SCSSA Optimization Process and Envelope Spectrum of Simulation Signal After the Proposed Method

Subsequently, SCSSA-MCKD deconvolution processing is performed with parameters *[L,T,M]* = [885,123,6] and the best fitness value of 5.0574. The results are shown in Fig.5. It is clearly observed that the envelope spectrum displays very prominent inner ring fault frequencies and their harmonics (2~9 times frequency), indicating that the proposed method is highly effective for simulating inner ring fault signals.

5. Experimental signal analysis

5.1. Verification with public dataset

To validate the effectiveness and feasibility of the proposed method, we used test data from the Case Western Reserve University Bearing Data Center [19]. The test setup consists of a drive motor, a controller, a torque sensor, and a test bearing. A deep groove ball bearing of model SKF6203 was installed at the motor fan end, and an accelerometer was magnetically attached to the motor housing. A defect with a diameter of 0.5334 mm and a depth of 0.2794 mm was created on the inner ring of the bearing using electrical discharge machining. During the test, the motor load was 1.49 kW, and the sampling frequency was 12 kHz. Vibration data from the drive end was selected, with 12,000 sampling points set. Fig.8 shows the time-domain waveform and envelope spectrum of the collected vibration signal. The time-domain waveform exhibits complex impact components, while the envelope spectrum clearly shows rotational frequency components with many harmonic frequencies, making it difficult to directly identify fault characteristics. The calculated rotational frequency f_r=29.17Hz, and the inner ring fault frequency is f_i=144.30Hz.

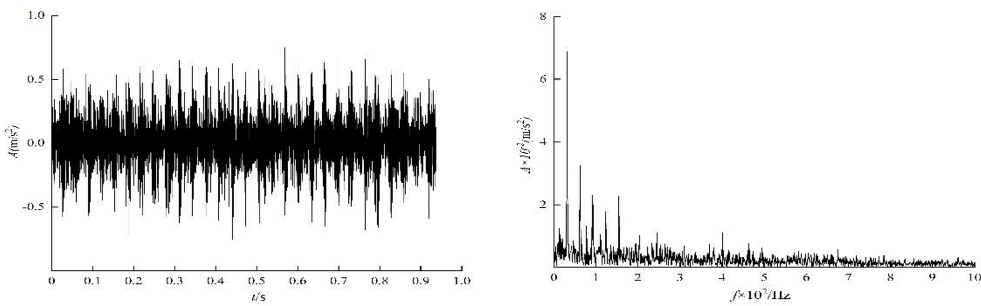

(a) Original Time-Domain Waveform of Public Dataset Signal
(b) Original Envelope Spectrum of Public Dataset Signal

Figure 4. Data Waveform and Envelope Spectrum of Open Data Set

First, ACMD is applied to decompose the signal, resulting in 8 intrinsic mode functions (IMFs). The Gini Index is calculated for each component. Based on the Gini Index ranking and the time-domain waveforms of the IMFs, the optimal component is determined to be IMF2.

Table 1. Values of Gini Coefficients of the Components of the Open Data Set

Component Number	Gini Coefficient
1	0.5837
2	0.6536
3	0.5389
4	0.5230
5	0.5157
6	0.4821
7	0.5122
8	0.5324

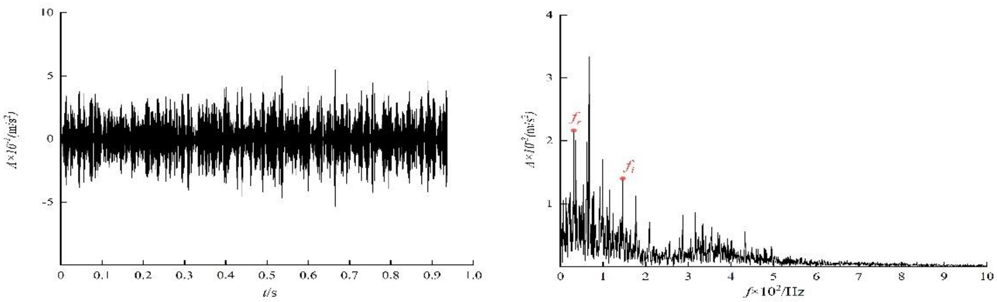

(a) Time Domain Waveform of the Optimal Component
(b) Envelope Spectrum of the Optimal Component

Figure 5. Time Domain Waveform and Envelope Spectrum of Optimal Component of Exposed Data Set

According to Fig.5, which shows the time domain waveform and envelope spectrum of the optimal component of the open data set, compared to Fig.4, there is a noticeable reduction in random interference impact components, and it reveals the characteristics of the time domain waveform when a bearing inner ring fault occurs. Furthermore, the envelope spectrum prominently displays the characteristic frequency of the bearing inner ring fault, indicating possible inner ring damage.

After substituting the optimal component into the MCKD algorithm optimized by SCSSA, the combined parameters *[L,T,M]* are [298,85,5]. Set the MCKD algorithm filter length parameter L=298, deconvolution period T=85, displacement parameter M=5, and the optimal fitness value is 10.5641. Reintroduce these parameters back into the algorithm to obtain the time domain waveform and envelope spectrum of the optimal component after deconvolution, as shown in Fig.9(b,c).

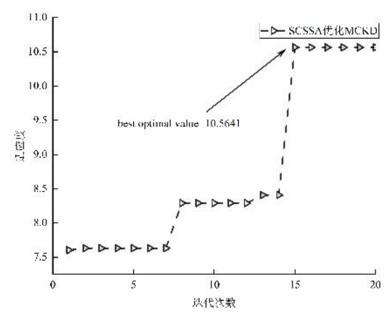

(a) SCSSA Optimization Process

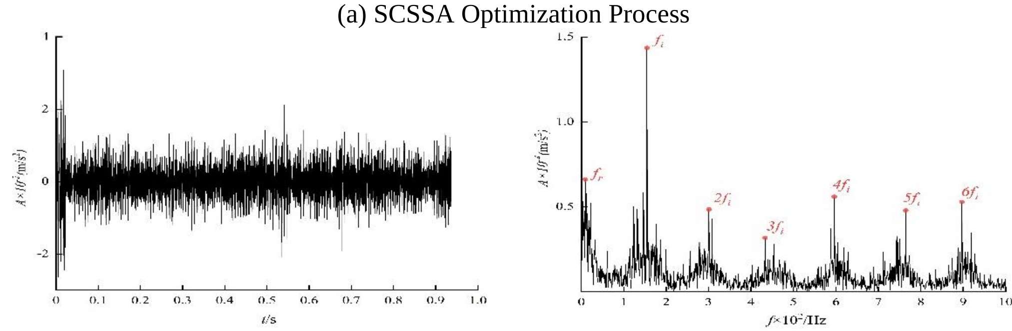

(b) Time Domain Waveform of the Optimal Component of the Open Data Set After the Proposed Method
(c) Envelope Spectrum of the Optimal Component of the Open Data Set After the Proposed Method

Figure 6. Time Domain Waveform and Envelope Spectrum of the Open Data Set After the Proposed Method

Using the SCSSA-MCKD filter to process the optimal component, the time domain waveform and envelope spectrum shown in Fig.8 are obtained. Compared to the ACMD decomposition results in Fig.5, after deconvolution, the periodic impacts in the signal's time domain waveform are more pronounced. The signal's envelope spectrum exhibits distinct characteristic frequencies of the inner ring fault and its 2~6 harmonics, without the interference of rotational frequencies that could affect the fault type judgment. This confirms that the bearing has an inner ring fault.

5.2. Verification on the dynamic performance test bench of railway freight car bearings

5.2.1. Test equipment and basic parameters of bearings

Railway freight car bearings are one of the most important components in the running gear of trains, primarily consisting of the outer ring, inner ring, cage, and rolling elements [20]. The main function of the inner ring is to support and position the rolling elements, typically installed on the shaft, ensuring good fit between the shaft and the inner ring, allowing the shaft to rotate on the inner ring.

Figure 7. Structure Diagram of Railway Truck Bearing

To verify the effectiveness and generalizability of the proposed method, a dynamic performance test bench for railway freight car bearings was selected for vibration signal acquisition, as shown in Fig.10. The test bearing is a 353130B double-row tapered roller bearing, with basic parameters listed in Table 2. Two INV9822 vibration sensors were mounted on the surface of the bearing's outer ring in a right-angle distribution. During the test, real-time data acquisition was conducted using the DASP module of the Dongfang Vibration Data Acquisition Instrument [21]. The sampling duration was 60 seconds, the sampling frequency was 25.6 kHz, and the rotational speed was 1000 r/min. By calculation, the rotational frequency of the bearing inner ring f_r=16.67Hz, and the theoretical fault characteristic frequency f_i=98.6Hz.

(a) Dynamic Performance Test Bench for Railway Bearings
(b) Vibration Sensor Positions

Figure 8. Dynamic Performance Test Bench of Railway Freight Car Bearing

Table 2. Test Bearing Size Table

Model	353130B
Inner diameter (mm)	150
Outer diameter (mm)	250
Outer ring height (mm)	160
Number of rollers per half set	11
Contact angle (°)	10

5.2.2. Inner ring fault analysis

The time domain waveform and envelope spectrum of the original signal for the inner ring fault are shown in Fig. 9. The impact vibration signal is intertwined with the noise signal, making it difficult to clearly distinguish the fault impact signal. In the envelope spectrum, there are multiple high-amplitude and chaotic spectral lines, making it impossible to accurately identify the characteristic frequency of the inner ring fault and to determine whether there is an inner ring fault in the rolling bearing.

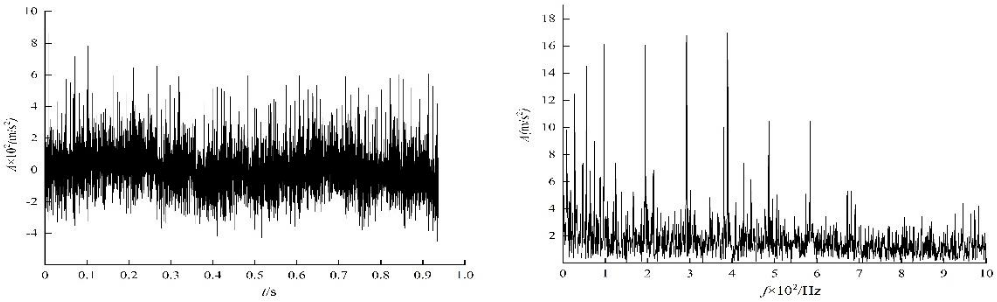

(a) Time Domain Waveform of the Original Signal of the Measured Data Set
(b) Envelope Spectrum of the Measured Data Set Signal

Figure 9. Data Waveform and Envelope Spectrum of Measured Data Set

First, the original signal was decomposed using ACMD, resulting in eight components (IF1-IF8) as shown in Fig. 10. The component with the largest Gini coefficient, IMF6, was selected as the optimal component.

Table 3. Values of Gini coefficients of measured dataset components

Component number	Gini coefficient
1	0.54714
2	0.47374
3	0.64801
4	0.52852
5	0.75556
6	0.85384
7	0.55352
8	0.61824

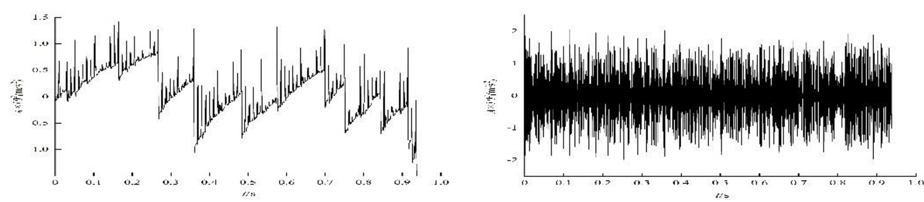

(a) IMF1 (b) IMF2

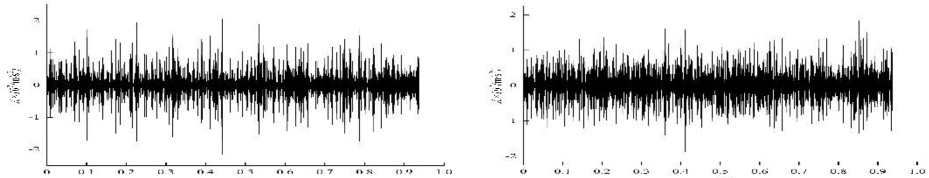

(c) IMF3 (d) IMF4

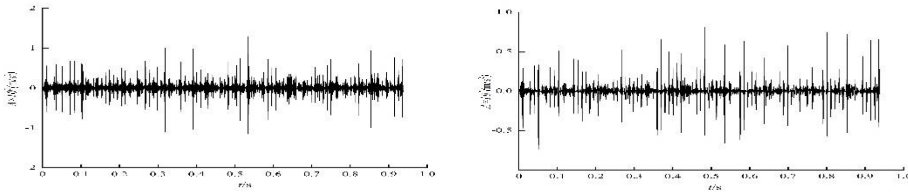

(e) IMF5 (f) IMF6

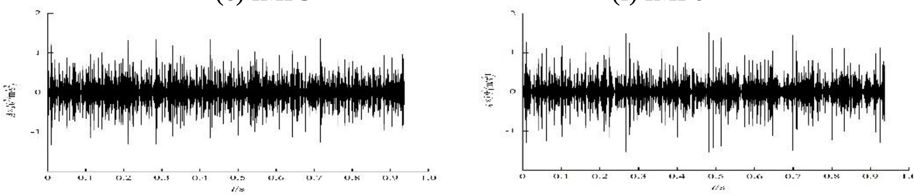

(g) IMF7 (h) IMF8

Figure 10. Component Waveform of Measured Data Set Decomposed by ACMD

The time domain waveform and envelope spectrum of the optimal component are shown in Fig.11. Compared to Fig.9, Fig.11 shows a significant reduction in random interference impact components and displays the characteristic waveform of bearing outer ring fault in the time domain. Additionally, the characteristic frequency of the bearing inner ring fault is highlighted in the envelope spectrum, indicating a potential inner ring damage in the bearing.

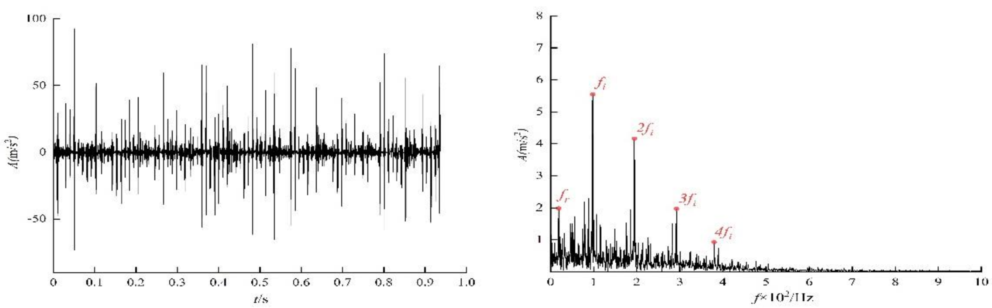

(a) Time Domain Waveform of the Optimal Component of the Measured Data Set
(b) Envelope Spectrum of the Optimal Component of the Measured Data Set

Figure 11. Optimal Component Waveform and Envelope Spectrum of Measured Data

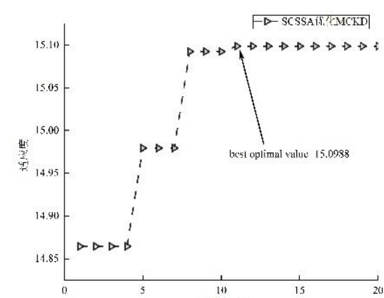

(a) SCSSA Optimization Process

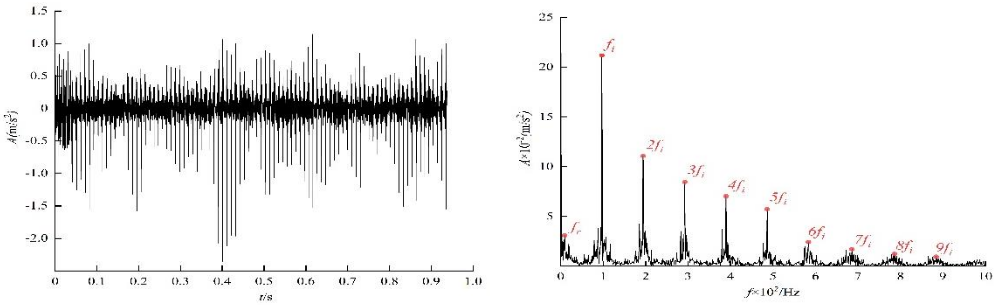

(b) Time Domain Waveform of the Optimal Component After the Proposed Method
(c) Envelope Spectrum of the Optimal Component After the Proposed Method

Figure 12. Time Domain Waveform and Envelope Spectrum of the Measured Data Set After the Proposed Method

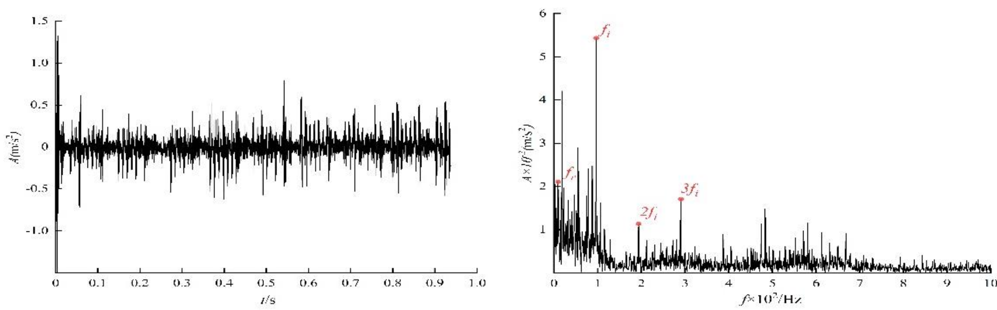

(a) Time Domain Waveform After ACMD-MCKD Processing
(b) Envelope Spectrum After ACMD-MCKD Processing

Figure 13. Time Domain Waveform and Envelope Spectrum of Measured Data Set After ACMD-MCKD Processing

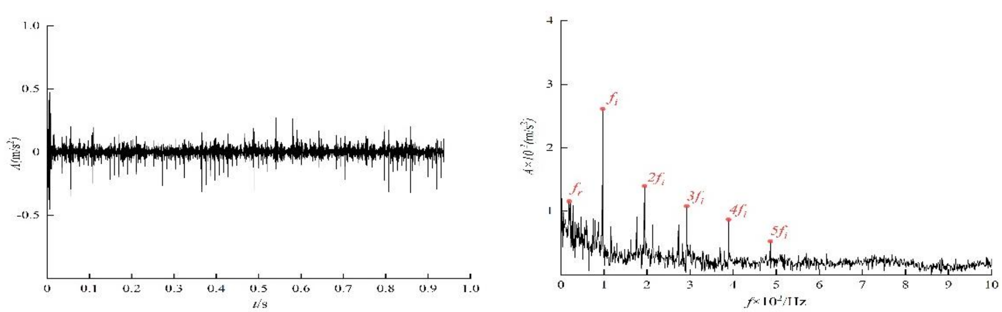

(a) Time Domain Waveform After PSO-MCKD Processing
(b) Envelope Spectrum After PSO-MCKD Processing

Figure 14. Time Domain Waveform and Envelope Spectrum of Measured Data Set After PSO-MCKD Processing

After optimizing the MCKD with the SCSSA algorithm, the parameters *[L,T,M]* were obtained as [534, 131, 4], and the best fitness value was 15.0988. The time domain waveform and envelope spectrum of the optimal component after deconvolution are shown in Fig. 12(b, c).

Comparing Fig. 12 with the time domain waveform and envelope spectrum after ACMD decomposition in Fig. 11, it can be seen that the periodic impacts in the deconvoluted signal's time domain waveform are more pronounced. Additionally, the envelope spectrum of the signal clearly reveals the inner ring fault characteristic frequencies and their (2–9 times frequency components), without interference from the rotational frequency components in fault type identification. Compared to the results after processing with the method shown in Fig. 13, the fault characteristic harmonic frequency lines in Fig. 14 are clearer, indicating a better extraction of fault characteristics and demonstrating the necessity of SCSSA for adaptive optimization of MCKD parameters. Furthermore, the results from the PSO-MCKD method in Fig. 14 show that the fault characteristic harmonic frequency lines in Fig. 12 are more distinct and accurate, providing a better extraction of fault characteristics. This further demonstrates that, under the same conditions, SCSSA optimization of MCKD offers superior inner ring fault diagnosis performance. During the iteration process, SCSSA converged in 12 iterations, whereas PSO required 20 iterations to converge, indicating that SCSSA converges faster and requires less time per iteration, highlighting the higher efficiency of SCSSA in optimizing the MCKD fault diagnosis process. Therefore, this underscores the necessity and high adaptability of SCSSA for MCKD optimization, and confirms the occurrence of inner ring faults in the bearing.

The analysis of the 353130B bearing test data from the railway freight car dynamic performance test bench, based on the inner ring fault simulation signal and open data set validation, further proves the effectiveness and applicability of the proposed method in extracting rolling bearing fault characteristics under strong noise backgrounds.

6. Conclusion

To address the challenge of extracting rolling bearing fault features under strong background noise conditions, this paper proposes the ACMD-SCSSA-MCKD fault diagnosis method for fault extraction and diagnosis in noisy environments.

The effectiveness, robustness, and generalization capability of the proposed method have been validated through simulation signals, the Case Western Reserve University bearing experiment center dataset, and the analysis of 353130B bearing test data from railway freight cars.

(1) The ACMD method, based on the Gini coefficient signal reconstruction principle, adaptively processes the original signal, improving the signal-to-noise ratio. Compared to traditional VMD and EMD methods, this approach is adaptive and does not require prior knowledge of the number of components, which helps avoid issues related to manual parameter setting and improves fault diagnosis accuracy.

(2) Compared to traditional Particle Swarm Optimization (PSO) algorithms, which optimize the L and T parameters in MCKD, this paper achieves optimal parameters L, T, and M through the SCSSA algorithm’s adaptive optimization process. This reduces errors potentially introduced by manual parameter settings, effectively enhances fault characteristic recognition, and mitigates interference from spurious frequencies, thereby improving the method’s adaptability.

(3) The results indicate that the ACMD-SCSSA-MCKD method can clearly extract hidden periodic fault impact signals under complex background noise conditions, providing accurate fault characteristic information and validating its theoretical and practical effectiveness. Future research could extend this method with deep learning to apply it more accurately to critical components like rolling bearings in railway freight cars.

References

[1] Yang, J., Junguo, W., & Zhao, Y. (2023). Non-linear dynamics and stability of the rolling bearing–axle coupling system of a railway freight wagon with changes in axle rotating speed. *Engineering Computations, 40*(1).

[2] Su, W., Wang, F., Zhang, Z., et al. (2010). Application of EMD denoising and spectral kurtosis methods in early fault diagnosis of rolling bearings. *Vibration and Shock, 29*(03), 18-21. https://doi.org/10.13465/j.cnki.jvs.2010.03.046

[3] Li, J., Zhou, D., & Si, X., et al. (2012). A review of micro-fault diagnosis methods. *Control Theory & Applications, 29*(12), 1517-1529.

[4] Dragomiretskiy, K., & Zosso, D. (2014). Variational mode decomposition. *IEEE Transactions on Signal Processing, 62*(3), 531-544.

[5] Chen, S., Peng, Z., & Zhou, P. (2020). A review of signal decomposition and its application in mechanical fault diagnosis. *Journal of Mechanical Engineering, 56*(17), 91-107.

[6] Shiqian, C., Xingjian, D., Zhike, P., et al. (2017). Nonlinear chirp mode decomposition: A variational method. *IEEE Transactions on Signal Processing, 65*(22).

[7] Tang, G., & Wang, X. (2015). Adaptive maximum correlated kurtosis deconvolution method and its application in early fault diagnosis of bearings. *Proceedings of the CSEE, 35*(06), 1436-1444. https://doi.org/10.13334/j.0258-8013.pcsee.2015.06.019

[8] Li, A., Quan, L., & Cui, G., et al. (2022). Sparrow search algorithm integrated with cosine and Cauchy mutations. *Computer Engineering and Applications*, *58*(03), 91-99.

[9] Zhang, J., Zhang, J., Zhong, M., et al. (2020). Weak fault diagnosis of fan bearings based on the PSO-VMD-MCKD method. *Vibration, Testing & Diagnosis, 40*(02), 287-296+418. https://doi.org/10.16450/j.cnki.issn.1004-6801.2020.02.011

[10] Xue, J. (2021). Research and application of a novel swarm intelligence optimization technique [Doctoral dissertation, Donghua University]. https://doi.org/10.27012/d.cnki.gdhuu.2020.000178

[11] Lu, S. (2015). Research on weak signal detection model and its applications based on stochastic resonance [Doctoral dissertation, University of Science and Technology of China].

[12] Singer, B., Zhong, Q., & Li, Z., et al. (2022). Autonomous recognition method for early faults in train axle box bearings based on Ginigram and CHMR. *China Railway Science, 43*(02), 104-114.

[13] Shiqian, C., Kaiyun, W., Chao, C., et al. (2021). A two-level adaptive chirp mode decomposition method for railway wheel flat detection under variable-speed conditions. *Journal of Sound and Vibration, 498*, 115963.

[14] Hu, A., & Zhao, J. (2019). Rolling bearing multi-fault diagnosis based on adaptive maximum correlated kurtosis deconvolution. *Vibration and Shock, 38*(22), 171-177. https://doi.org/10.13465/j.cnki.jvs.2019.22.024

[15] Wang, X. (2017). Research on rolling bearing fault diagnosis methods based on vibration signal processing [Doctoral dissertation, North China Electric Power University (Beijing)].

[16] Dongjie, L., Mingyue, L., Liu, Y., et al. (2023). Rolling bearing fault diagnosis in strong noise background based on vibration signals. *Signal, Image and Video Processing, 18*(2).

[17] Xue, J., & Shen, B. (2020). A novel swarm intelligence optimization approach: Sparrow search algorithm. *Systems Science & Control Engineering, 8*(1), 22-34.

[18] Mao, Q., & Zhang, Q. (2021). Improved sparrow search algorithm integrated with Cauchy mutation and reverse learning. *Computer Science and Exploration, 15*(06), 1155-1164.
[19] Smith, A. W., & Randall, B. R. (2015). Rolling element bearing diagnostics using the Case Western Reserve University data: A benchmark study. *Mechanical Systems and Signal Processing, 64-65*, 100-131.
[20] Bingyan, C., Weihua, Z., Dongli, S., et al. (2023). Squared envelope sparsification via blind deconvolution and its application to railway axle bearing diagnostics. *Structural Health Monitoring, 22*(6), 3637-3658.
[21] Yuan, H., & Chen, G. (2007). Application of DASP technology in modern testing instrument platforms. *Journal of Electronic Measurement and Instrumentation, 21*(01), 53-56. https://doi.org/10.13382/j.jemi.2007.01.021